NASA
Technical
Paper
3353

August 1993

Final State Interactions and Inclusive Nuclear Collisions

Francis A. Cucinotta
and Rajendra R. Dubey

NASA

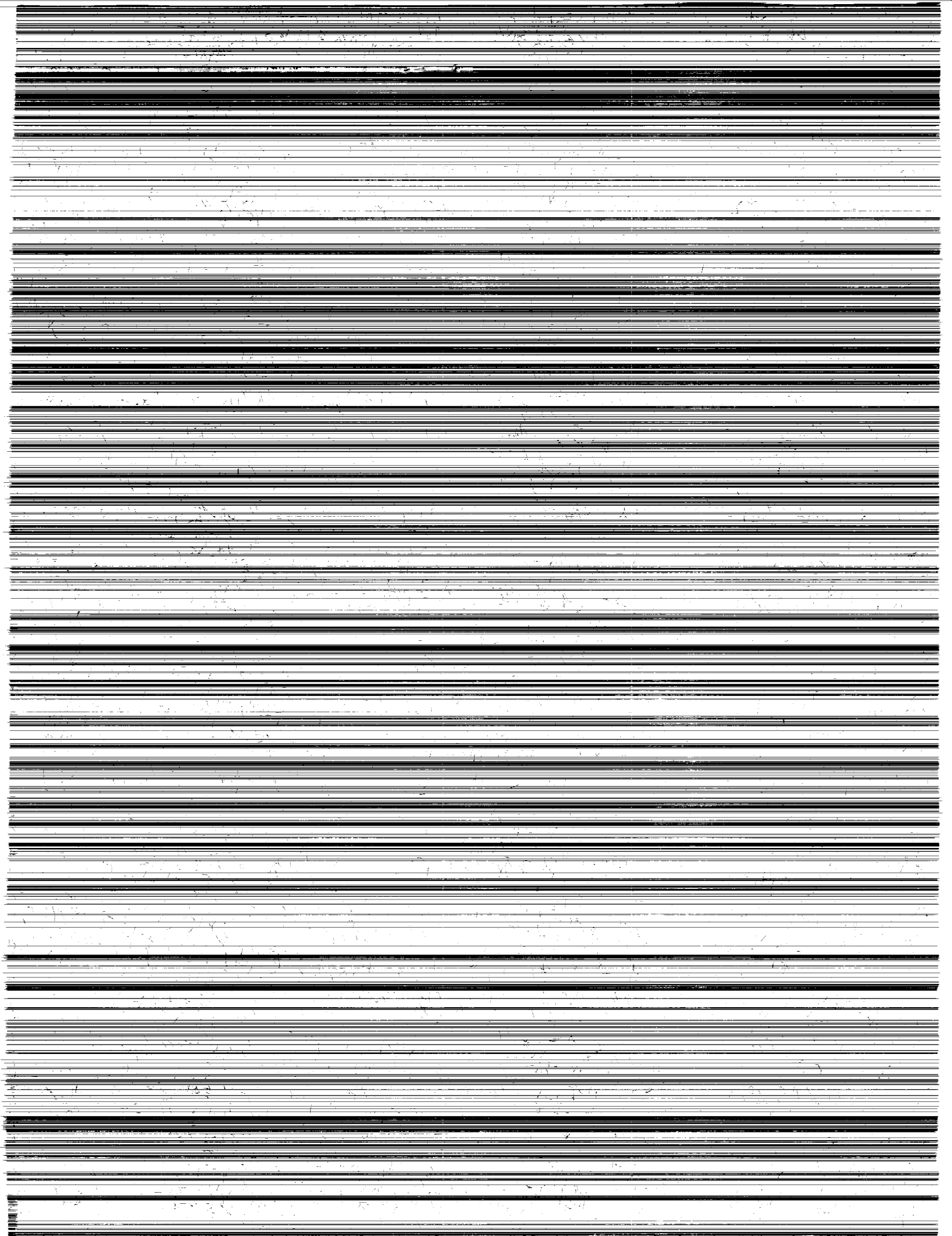

NASA Technical Paper 3353

1993

Final State Interactions and Inclusive Nuclear Collisions

Francis A. Cucinotta
Langley Research Center
Hampton, Virginia

Rajendra R. Dubey
Old Dominion University
Norfolk, Virginia

National Aeronautics and Space Administration
Office of Management
Scientific and Technical Information Program

Abstract

A scattering formalism is developed in a multiple scattering model to describe inclusive momentum distributions for high-energy projectiles. The effects of final state interactions on response functions and momentum distributions are investigated. Calculations for high-energy protons that include shell model response functions are compared with experiments.

Introduction

A realistic description of galactic cosmic ray transport through bulk shielding requires an extensive data base of nuclear interaction cross sections. (See ref. 1.) Traditionally, velocity-conserving interactions have been assumed for all ions with a mass number greater than one for easier numerical computations. (See ref. 1.) As transport algorithms become more accurate, this assumption will likely be removed; the result will be an increased need for nuclear data bases that include secondary particle spectra.

Previously (refs. 2 and 3), we developed a multiple scattering series to describe the energy loss spectra of fast ions in nuclear collisions. This multiple scattering series, which describes the quasi-elastic peak, was effectively summed by expressing the many-body response functions of the target as a convolution of the one-body response function through an energy shift approximation. For composite projectiles, incoherent corrections were shown to slightly reduce the cross section (refs. 2 and 3), when uncorrelated form factors were assumed. Multiple scattering effects were also shown to shift the position of the quasi-elastic peak considerably, which agrees with experiments. In references 2 and 3, a two-dimensional representation of the target response function was used in the eikonal formalism. In this paper we treat the longitudinal aspects of the response; however, we used the eikonal approximation to evaluate the cross section. In this paper we also focus on the final state interaction (FSI) between knocked-out target nucleons and the target recoil. A treatment of the FSI in inclusive scattering is important for understanding scaling phenomena (refs. 4–6) and transparency (refs. 7–9) in high-energy collisions as well as in the intranuclear cascade.

In inclusive scattering with fast ions, the projectile has left the scattering region before the FSI; thus, a simplified treatment of ion effects on the projectile wave function may be valid. Focusing on energy losses above low-lying collective states and below pion production thresholds, we consider ejectiles of the target using the approach of Horikawa et al. (ref. 10) for decomposition of the response function into elastic and inelastic FSI's. We then evaluate these terms by using the eikonal approximation to the Moller operator. Pauli exclusion effects are neglected in this preliminary treatment of the FSI. A rough estimate of exclusion effects is made from a medium, modified, two-body cross section. Proton projectiles are then compared with experiments based on the shell model in a harmonic oscillator basis. Included are the s, p, and d shells that allow calculations for targets up to ^{40}Ca.

Multiple Inelastic Collision Series

In the eikonal coupled channels (ECC) model (refs. 11–13), the matrix of scattering amplitudes for all possible projectile-target transitions is given by

$$\bar{\mathbf{f}}(\mathbf{q}) = \frac{ik}{2\pi}\widehat{Z}\int d^2b\; e^{i\mathbf{q}\cdot\mathbf{b}}\left\{e^{i\bar{\chi}(\mathbf{b})} - \bar{1}\right\} \tag{1}$$

where barred quantities represent matrices, $\mathbf{b}$ is the impact parameter vector, $\mathbf{q}$ is the momentum transfer vector, and k is the projectile-target relative wave number. In equation (1), $\widehat{Z}$ is an ordering operator for the z-coordinate that is necessary only when noncommuting two-body

interactions are considered. The eikonal phase elements are defined by matrix elements of arbitrary projectile-target states of the following operator:

$$\widehat{\chi}(\mathbf{b}) = \frac{1}{(2\pi)^2 k_{\rm NN}} \sum_{\alpha,j} \int_{-\infty}^{\infty} dz \int d^3q \; e^{i\mathbf{q}\cdot\boldsymbol{\eta}} \; e^{-i\mathbf{q}\cdot\mathbf{r}_\alpha} \; e^{i\mathbf{q}\cdot\mathbf{r}_j} f_{\rm NN}(\mathbf{q}) \tag{2}$$

where α and j label the projectile and target constituents, respectively; $\mathbf{r}$ is the internal nuclear coordinate; $\boldsymbol{\eta}$ is the projectile-target separation with $\boldsymbol{\eta} = (\mathbf{b}, z)$; $f_{\rm NN}$ is the nucleon-nucleon (NN) amplitude; and $k_{\rm NN}$ is the NN relative wave number.

When treating inelastic scattering, we assume that the off-diagonal terms in $\overline{\chi}$ (denoted by $\overline{\chi}_o$) are small compared with the diagonal ones, $\overline{\chi}_D$; then we expand $\bar{\mathbf{f}}$ in powers of $\overline{\chi}_o$ to

$$\bar{\mathbf{f}}(\mathbf{q}) = \frac{ik}{2\pi} \int d^2b \; e^{i\mathbf{q}\cdot\mathbf{b}} e^{i\overline{\chi}_D(\mathbf{b})} \sum_{m=1} \left\{ \frac{\left[i\overline{\chi}_o(\mathbf{b})\right]^m}{m!} \right\} \tag{3}$$

We also will make the assumption that all the diagonal terms are represented by the ground-state elastic phase χ. Using equation (3), we sum over target final states X (continuum) to find the inclusive angular distribution for the projectile when its mass remains unchanged as in

$$\left.\frac{d\sigma}{d\Omega}\right)_{\rm IN} = \frac{k^2}{(2\pi)^2} \int d^2b \; d^2b' \; e^{i\mathbf{q}\cdot(\mathbf{b}-\mathbf{b}')} \; e^{i\left[\chi(\mathbf{b})-\chi^\dagger(\mathbf{b}')\right]}$$
$$\times \sum_{X\neq 0} \sum_{m=1} \frac{1}{(m!)^2} < 0_P 0_T | \left[i\widehat{\chi}(\mathbf{b})\right]^m |0_P X >< X 0_P| \left[-i\widehat{\chi}^\dagger(\mathbf{b}')\right]^m |0_P 0_T > \tag{4}$$

Equation (4) only allows for a study of the momentum transfer spectra of the projectile. However, in any consideration of the projectile energy loss, energy conservation must be treated. Based on continuum states for the target final state, energy conservation leads to

$$\left.\frac{d^2\sigma}{d\Omega \; dE_{P'}}\right)_{\rm IN} = \frac{k^2}{(2\pi)^2} \int d^2b \; d^2b' \; e^{i\mathbf{q}\cdot(\mathbf{b}-\mathbf{b}')} \; e^{i\left[\chi(\mathbf{b})-\chi^\dagger(\mathbf{b}')\right]} \sum_{m=1}^{A_T} W_m(\mathbf{b}, \mathbf{b}', \omega) \tag{5}$$

and

$$\left.\frac{d\sigma}{dE_{P'}}\right)_{\rm IN} = \int d^2b \; e^{-2 \; {\rm Im} \; \chi(\mathbf{b})} \sum_{m=1}^{A_T} W_m(\mathbf{b}, \mathbf{b}, \omega) \tag{6}$$

where $E_{P'}$ is the energy of the projectile in the final state, ω is the projectile energy loss, and we define

$$W_m(\mathbf{b}, \mathbf{b}', \omega) = \frac{1}{(m!)^2} \int \prod_{j=1}^{m} \left[\frac{d\mathbf{k}_j}{(2\pi)^3}\right] \delta(E_f - E_i) < 0_P 0_T | \left[\widehat{\chi}(\mathbf{b})\right]^m |0_P \mathbf{k}_j >$$
$$\times < \mathbf{k}_j 0_P | \left[\widehat{\chi}^\dagger(\mathbf{b}')\right]^m |0_P 0_T > \tag{7}$$

where $\mathbf{k}_j$ is the wave number vector of a knocked-out target nucleon.

The inelastic collision series of equation (5) is expected to converge fairly rapidly. In the next section we consider the evaluation of this series for an uncorrelated target wave function.

Collision Terms in Plane Wave Approximation

We first consider the evaluation of the collision terms W_m using plane waves for the final continuum states of the target. The projectile motion is treated in the coherent approximation. (See ref. 1.) We consider a three-dimensional representation of the collision terms rather than just the transverse terms considered in references 2 and 3. The effects of correlations are not treated herein.

The first collision term is written

$$W_1\left(\mathbf{b},\mathbf{b}',\omega\right) = \frac{A_P^2 A_T}{(2\pi)^4 k_{\mathrm{NN}}^2}\int_{-\infty}^{\infty} dz \int_{-\infty}^{\infty} dz' \int d\mathbf{q}\, d\mathbf{q}'\, e^{i\mathbf{q}\cdot\boldsymbol{\eta}}\, e^{-i\mathbf{q}'\cdot\boldsymbol{\eta}'}$$

$$\times F(\mathbf{q})F(\mathbf{q}')f_{\mathrm{NN}}(\mathbf{q})f_{\mathrm{NN}}^{\dagger}(\mathbf{q}')\int \frac{d^3\mathbf{k}}{(2\pi)^3}\,\delta(\omega - E_{\mathbf{k}})G_{0_T\mathbf{k}}(\mathbf{q})\, G_{\mathbf{k}0_T}^{\dagger}(\mathbf{q}') \qquad (8)$$

where $G_{0_T\mathbf{k}}$ is the transition form factor of the target and A_P and A_T are the projectile and target mass numbers, respectively. It is helpful to change variables as

$$\boldsymbol{\alpha} = \frac{1}{2}(\mathbf{q}+\mathbf{q}') \qquad (9)$$

$$\boldsymbol{\beta} = \mathbf{q}-\mathbf{q}' \qquad (10)$$

$$\mathbf{x} = \mathbf{r}-\mathbf{r}' \qquad (11)$$

$$\mathbf{y} = \frac{1}{2}\,(\mathbf{r}+\mathbf{r}') \qquad (12)$$

Also,

$$\mathbf{R} = \boldsymbol{\eta}-\boldsymbol{\eta}' \qquad (13)$$

$$\mathbf{S} = \frac{1}{2}(\boldsymbol{\eta}+\boldsymbol{\eta}') \qquad (14)$$

with the transverse parts denoted $\mathbf{R}_\perp$ and $\mathbf{S}_\perp$, respectively. The first collision term is rewritten using equations (9)–(14) as

$$W_1\left(\mathbf{R}_\perp,\mathbf{S}_\perp,\omega\right) = \frac{A_P^2 A_T}{(2\pi)^4 k_{\mathrm{NN}}^2}\int dz\, dz'\, d^3\alpha\, d^3\beta\, e^{i\boldsymbol{\alpha}\cdot\mathbf{R}}\, e^{i\boldsymbol{\beta}\cdot\mathbf{S}}$$

$$\times A\left(\boldsymbol{\alpha}+\frac{\boldsymbol{\beta}}{2}\right)A^{\dagger}\left(\boldsymbol{\alpha}-\frac{\boldsymbol{\beta}}{2}\right)R_1(\boldsymbol{\alpha},\boldsymbol{\beta},\omega) \qquad (15)$$

where we have defined

$$A(\mathbf{q}) = F(\mathbf{q})f_{\mathrm{NN}}(\mathbf{q}) \qquad (16)$$

and

$$R_1(\boldsymbol{\alpha},\boldsymbol{\beta},\omega) = \int \frac{d^3k}{(2\pi)^3}\delta(\omega - E_{\mathbf{k}})G_{0\mathbf{k}}\left(\boldsymbol{\alpha}+\frac{\boldsymbol{\beta}}{2}\right)G_{\mathbf{k}0}^{\dagger}\left(\boldsymbol{\alpha}-\frac{\boldsymbol{\beta}}{2}\right) \qquad (17)$$

Introducing the Fourier transform pair

$$R_1(\boldsymbol{\alpha},\boldsymbol{\beta},\omega) = \int \frac{dt}{(2\pi)} e^{i\omega t} \widetilde{R}_1(\boldsymbol{\alpha},\boldsymbol{\beta},t) \tag{18}$$

and

$$\widetilde{R}_1(\boldsymbol{\alpha},\boldsymbol{\beta},t) = \int d\omega\ e^{-i\omega t} R_1(\boldsymbol{\alpha},\boldsymbol{\beta},\omega) \tag{19}$$

allows us to evaluate the energy-conserving delta function in equation (17). (See ref. 14.) For the target nucleons, we assume that

$$E_{\mathbf{k}} = \frac{\mathbf{k}^2}{2m_N} + \epsilon_{B_1} \tag{20}$$

where m_N is the nucleon mass, ϵ_{B_1} is the binding energy, and equation (19) is

$$\begin{aligned}\widetilde{R}_1(\boldsymbol{\alpha},\boldsymbol{\beta},t) = \int \frac{d\mathbf{k}}{(2\pi)^3}\, d\mathbf{x}\, d\mathbf{y}\ e^{-i\epsilon_{B_1} t}\ e^{-ik^2 t/2m_N}\ e^{i\mathbf{k}\cdot\mathbf{x}} \\ \times e^{i\boldsymbol{\alpha}\cdot\mathbf{x}}\ e^{i\boldsymbol{\beta}\cdot\mathbf{y}}\ \rho\left(\mathbf{y}+\frac{\mathbf{x}}{2}, \mathbf{y}-\frac{\mathbf{x}}{2}\right)\end{aligned} \tag{21}$$

where the density matrix is $\rho(\mathbf{r},\mathbf{r}')$ and is defined by

$$\rho(\mathbf{r},\mathbf{r}') = \Phi(\mathbf{r})\ \Phi^{\dagger}(\mathbf{r}') \tag{22}$$

and Φ is the ground-state single-particle wave function. We then find

$$R_1(\boldsymbol{\alpha},\boldsymbol{\beta},\xi) = \frac{m_N \xi_1}{(2\pi)^2} \int d^3x\, d^3y\, e^{i\boldsymbol{\alpha}\cdot\mathbf{x}}\, e^{i\boldsymbol{\beta}\cdot\mathbf{y}}\ j_o(\xi_1 x) \rho\left(\mathbf{y}+\frac{\mathbf{x}}{2}, \mathbf{y}-\frac{\mathbf{x}}{2}\right) \Theta\left(\omega - \epsilon_{B_1}\right) \tag{23}$$

where j_o is a spherical Bessel function, Θ is the unit step function, and

$$\xi_1 = \sqrt{2m_N\left(\omega - \epsilon_{B_1}\right)} \tag{24}$$

The higher order terms are more difficult to treat because of the enumeration of projectile and target intermediate states. A first approximation is to assume that the projectile remains in the ground state throughout the collision (coherent projectile approximation).

Using similar coordinate changes as described above, we find the mth-order collision term as

$$\begin{aligned}W_m(\mathbf{R}_\perp,\mathbf{S}_\perp,\omega) = \frac{A_P^{2m} A_T^m}{(m!)^2 k_{\mathrm{NN}}^{2m} (2\pi)^{(2m+2)}} \int dz\, dz' \int \prod_{j=1}^{m} \Big[d^3\alpha_j\, d^3\beta_j \\ \times e^{i\boldsymbol{\alpha}_j\cdot\mathbf{R}}\, e^{i\boldsymbol{\beta}_j\cdot\mathbf{S}} A_j\left(\boldsymbol{\alpha}_j+\frac{\boldsymbol{\beta}_j}{2}\right) A_j^{\dagger}\left(\boldsymbol{\alpha}_j-\frac{\boldsymbol{\beta}_j}{2}\right)\Big] \\ \times R_m(\boldsymbol{\alpha}_1,\ldots,\boldsymbol{\alpha}_m,\boldsymbol{\beta}_1,\ldots,\boldsymbol{\beta}_m,\omega)\end{aligned} \tag{25}$$

where

$$R_m(\boldsymbol{\alpha}_1,\ldots,\boldsymbol{\alpha}_m,\boldsymbol{\beta}_1,\ldots,\boldsymbol{\beta}_m,\omega) = \frac{m_N}{2}\left(\frac{1}{2\pi}\right)^{3m/2}\int\prod_{j=1}^{m}\Bigg[d^3x_j\; d^3y_j\; e^{i\boldsymbol{\alpha}_j\cdot\mathbf{x}_j}\; e^{i\boldsymbol{\beta}_j\cdot\mathbf{y}_j} \times \rho\left(\mathbf{y}_j+\frac{\mathbf{x}_j}{2},\mathbf{y}_j-\frac{\mathbf{x}_j}{2}\right)\Bigg]\frac{\xi_m^{3m/2-1}}{\left(\sum_j x_j^2\right)^{3m/4-1/2}} \times J_{3m/2-1}\left[\sqrt{2m_N\left(\omega-\epsilon_{B_m}\right)\sum_{j=1}x_j^2}\right]\Theta\left(\omega-\epsilon_{B_m}\right) \quad (26)$$

where $R_m = 0$ for $\omega < \epsilon_{B_m}$. The solutions for the mth-order terms in equation (26) result from the Fourier transform of the temporal response. Because we keep the longitudinal momentum transfer in the response (as opposed to the approach of cylindrical geometry in references 2 and 3), the order of the Bessel function in R_m differs from references 2 and 3. For forward-peaked wave functions, we approximate

$$R_m(\boldsymbol{\alpha}_1,\ldots,\boldsymbol{\alpha}_m,\boldsymbol{\beta}_1,\ldots,\boldsymbol{\beta}_m,\omega) \cong C_m(\omega-\epsilon_{B_m})^{m-1}\prod_{j=1}^{m}R_1\left(\boldsymbol{\alpha}_j,\boldsymbol{\beta}_j,\frac{\xi_m}{\sqrt{m}}\right)+O\left(\xi_j^4\; x_j^4\right) \quad (27)$$

such that

$$W_m(\mathbf{R}_\perp,\mathbf{S}_\perp,\omega) = \frac{C_m(\omega-\epsilon_{B_m})^{m-1}}{(m!)^2}\left[W_1\left(\mathbf{R}_\perp,\mathbf{S}_\perp,\frac{\xi_m}{\sqrt{m}}\right)\right]^m \quad (28)$$

where $C_1 = 1$, $C_2 = \frac{\pi}{4}$, $C_3 = \frac{\pi}{105}$, and $C_4 = \frac{\pi^2}{240}$. Equation (27) is found by considering the Taylor series for $J_{3m/2-1}$. The effective energy shift in equation (27) for the $m > 2$ approximation and the coefficients C_m differ from references 2 and 3 because of the longitudinal contributions to R_m that are included here. We then have for the energy loss spectra (eq. (5)) in a coherent projectile model,

$$\left.\frac{d^2\sigma}{d\Omega\; dE_{P'}}\right)_{\text{IN}} = \frac{k^2}{(2\pi)^2}\int d^2R\; d^2S\; e^{i\mathbf{q}\cdot\mathbf{R}_\perp}\; e^{i[\chi(\mathbf{R}_\perp+\mathbf{S}_\perp/2)-\chi^\dagger(\mathbf{R}_\perp-\mathbf{S}_\perp/2)]} \times\sum_{m=1}^{A_T}\frac{C_m(\omega-\epsilon_{B_m})^{m-1}}{(m!)^2}\left[W_1\left(\mathbf{R}_\perp,\mathbf{S}_\perp,\frac{\xi_m}{\sqrt{m}}\right)\right]^m \quad (29)$$

and

$$\frac{d\sigma}{dE_{P'}} = \int d^2S\; e^{-2\;\text{Im}\;\chi(S_\perp)} \times\sum_{m=1}^{A_T}\frac{C_m(\omega-\epsilon_{B_m})^{m-1}}{(m!)^2}\left[W_1\left(0,\mathbf{S}_\perp,\frac{\xi_m}{\sqrt{m}}\right)\right]^m \quad (30)$$

The coherent approximation assumes that the projectile remains in the ground state throughout the scattering. The leading-order correction to the coherent terms occurs in the collision term W_2 and corresponds to the following replacement of W_2 from references 2 and 3:

$$\begin{aligned} & A_P^4 F\left(\alpha_1+\frac{\beta_1}{2}\right) F\left(\alpha_1-\frac{\beta_1}{2}\right) F\left(\alpha_2+\frac{\beta_2}{2}\right) F\left(\alpha_2-\frac{\beta_2}{2}\right) \\ & \rightarrow A_P^2\left\{\left[F(2\alpha_1)+(A_P-1)\ F\left(\alpha_1+\frac{\beta_1}{2}\right)\ F\left(\alpha_1-\frac{\beta_2}{2}\right)\right]\right. \\ & \left.\times\left[F(2\alpha_2)+(A_P-1)\ F\left(\alpha_2+\frac{\beta_2}{2}\right)\ F\left(\alpha_2-\frac{\beta_2}{2}\right)\right]\right\} \end{aligned} \tag{31}$$

which follows from using closure on the projectile intermediate states. Physically, equation (31) allows the projectile to dissociate in the intermediate state. Further modifications are necessary when correlation effects are treated.

Final State Interactions

The target transition form factors will describe the effects of the FSI between the unobserved ejected nucleons and the recoiling target nucleus. We now consider these effects using the eikonal form of the optical model. Because the measurement is of the fast primary, we expect the details of the FSI on the primary wave function to be small. Therefore, we will introduce several approximations to obtain a tractable solution.

The transition form factor of the target appearing in the first-order response is given by

$$G_{0_T\mathbf{k}_1}(\mathbf{q}) = < 0_T \mid e^{i\mathbf{q}\cdot\mathbf{r}} \mid \psi_{\mathbf{k}_1}^{(-)} > \tag{32}$$

where $\psi_{\mathbf{k}_1}^{(-)}$ is the outgoing scattering state. With the Moller operator $\widehat{\Omega}_{\mathbf{k}_1}^{(-)}$, the transition form factor is written using plane-wave states as (ref. 4)

$$G_{0_T\mathbf{k}_1}(\mathbf{q}) = < 0_T \mid e^{i\mathbf{q}\cdot\mathbf{r}}\ \widehat{\Omega}_{\mathbf{k}_1}^{(-)} \mid \mathbf{k}_1\ > \tag{33}$$

The Moller operator is related to the Green function $\widehat{g}_o^{(-)}$ and to the transition operator $\widehat{T}$ as

$$\widehat{\Omega}_{\mathbf{k}_1}^{(-)} = 1 + \widehat{g}_o^{(-)}\widehat{T} \tag{34}$$

Using equations (33) and (34), we can separate the first-order response function into three terms corresponding to the plane-wave response, elastic distortion in the FSI, and inelastic reaction in the FSI (cascade). Thus,

$$R_1(\mathbf{q},\mathbf{q}',\omega) = R_1^{\mathrm{PW}} + R_1^{\mathrm{DW}} + R_1^{\mathrm{IN}} \tag{35}$$

The plane-wave term was described above. For the DW term, we have

$$\begin{aligned} R_1^{\mathrm{DW}} = & \int \frac{d^3k_1}{(2\pi)^3}\,\delta\left(\omega-E_{\mathbf{k}_1}\right)\left[< 0_R \mid e^{i\mathbf{q}\cdot\mathbf{r}}\ \widehat{g}_o^{(-)}\widehat{T}\mid \mathbf{k}_1 >< \mathbf{k}_1 \mid e^{-i\mathbf{q}'\cdot\mathbf{r}'}\mid 0_R >\right. \\ & \left. + < 0_R \mid e^{i\mathbf{q}\cdot\mathbf{r}} \mid \mathbf{k}_1 >< \mathbf{k}_1 \mid \widehat{g}_o^{(-)\dagger}\widehat{T}^\dagger\ e^{-i\mathbf{q}'\cdot\mathbf{r}'}\mid 0_R >\right] \end{aligned} \tag{36}$$

where $|0_R>$ is the ground-state wave function of the recoil nucleus. The cascade term describes a new inelastic collision series of the ejected nucleon with $\mathbf{k}_1$ reacting on the target recoil given by

$$R_1^{\mathrm{IN}} = \sum_{\ell=2}^{A_T} \int \frac{d^3k_1}{(2\pi)^3} \prod_{j=2}^{\ell} \left[\frac{d^3k_j}{(2\pi)^3}\right] \delta\left(\omega - E_{\mathbf{k}_1} - \sum_{j=2}^{\ell} E_{\mathbf{k}_j}\right)$$
$$\times < 0_R \mid e^{i\mathbf{q}\cdot\mathbf{r}}\, \widehat{g}_o^{(-)}\, \widehat{T} \mid \mathbf{k}_1 \prod_{j=2}^{\ell} \mathbf{k}_j >$$
$$\times < \mathbf{k}_1 \prod_{j=2}^{\ell} \mathbf{k}_j \mid \widehat{g}_o^{(-)\dagger} \widehat{T}^{\dagger}\, e^{-i\mathbf{q}'\cdot\mathbf{r}'} \mid 0_R > \tag{37}$$

We next consider the evaluation of formal equations (36) and (37) using the eikonal form of the optical model.

In the optical model (refs. 5–7), the Moller operator is expressed by the matrix

$$\overline{\mathbf{\Omega}}_{\mathbf{k}_1}^{(-)} = e^{i\overline{\chi}_R^{(-)}(\mathbf{s},z)} \tag{38}$$

where $\mathbf{s}$ denotes the transverse component of $\mathbf{r}$ and the subscript R indicates the coupling phases for the recoil system with matrix elements

$$\chi_R^{(-)} = \frac{(A_T - 1)}{(2\pi)^2 k_{\mathrm{NN}}} \int_z^{+\infty} dz \int d\mathbf{q}\; e^{i\mathbf{q}\cdot\mathbf{r}}\, G_{0_T\mathbf{k}_1}(\mathbf{q}) f_{\mathrm{NN}}(\mathbf{q}) \tag{39}$$

where the energy dependence of $\chi_R^{(-)}$ is determined by $\mathbf{k}_1$ rather than by the beam energy.

The diagonal part of $\overline{\mathbf{\Omega}}_{\mathbf{k}_1}^{(-)}$ determines the PW and DW response terms that we combine as

$$R_1^{\mathrm{EL}}(\mathbf{q},\mathbf{q}',\omega) = R_1^{\mathrm{PW}}(\mathbf{q},\mathbf{q}',\omega) + R_1^{\mathrm{DW}}(\mathbf{q},\mathbf{q}',\omega) \tag{40}$$

If we neglect incoherent contributions to the elastic distortion, we have

$$R_1^{\mathrm{EL}}(\mathbf{q},\mathbf{q}',\omega) = \int \frac{d^3k_1}{(2\pi)^3}\, \delta\left(\omega - E_{\mathbf{k}_1}\right) \int d\mathbf{r}\; d\mathbf{r}'\; e^{i\mathbf{q}\cdot\mathbf{r}}\; e^{-i\mathbf{q}'\cdot\mathbf{r}'}$$
$$\times\, e^{-i\mathbf{k}_1(\mathbf{r}-\mathbf{r}')} \rho\left(\mathbf{r},\mathbf{r}'\right) \exp\left\{ i\left[\chi_R^{(-)}\left(\mathbf{s},z\right) - \chi_R^{(-)\dagger}\left(\mathbf{s}',\mathbf{z}'\right)\right]\right\} \tag{41}$$

Expanding the phase of the distorted wave in equation (41) about $\mathbf{r} - \mathbf{r}' = 0$ and keeping only the first term were shown to provide accurate approximations for the distorted wave in reference 15 and are used here. Thus,

$$R_1^{\mathrm{EL}}(\boldsymbol{\alpha},\boldsymbol{\beta},\omega) \cong \int \frac{d^3k}{(2\pi)^3}\, \delta\left(\omega - E_{\mathbf{k}}\right) \int d^3x\; d^3y\; e^{i\boldsymbol{\alpha}\cdot\mathbf{x}}\; e^{i\boldsymbol{\beta}\cdot\mathbf{y}}$$
$$\times\, e^{i\mathbf{k}\cdot\mathbf{x}} \rho\left(\mathbf{y} + \frac{\mathbf{x}}{2}, \mathbf{y} - \frac{\mathbf{x}}{2}\right)\; e^{-2\ \mathrm{Im}\ \chi_R^{(-)}(\mathbf{y})} \Theta\left(\omega - \epsilon_{B_1}\right) \tag{42}$$

The calculation of $\chi_R^{(-)}$ is described in the appendix.

We make one further approximation by noting that the two-body parameters in $\chi_R^{(-)}$ change smoothly with the energy loss and provide the only dependence on $\mathbf{k}_1$ for this phase. Thus, we write

$$R_1^{\rm EL}\ (\mathbf{q},\mathbf{q}',\omega) = \frac{m_N\xi_1}{(2\pi)^2}\int d^3x\ d^3y\ e^{i\boldsymbol{\alpha}\cdot\mathbf{x}}\ e^{i\boldsymbol{\beta}\cdot\mathbf{y}}\ j_o(\boldsymbol{\xi}_1 x)\Theta\left(\omega-\epsilon_{B_1}\right)$$
$$\times\ \rho\left(\mathbf{y}+\frac{\mathbf{x}}{2}\right)\left(\mathbf{y}-\frac{\mathbf{x}}{2}\right)\ e^{-2\ {\rm Im}\ \chi_R^{(-)}(\mathbf{y})} \tag{43}$$

with the effective energy used for evaluating $\chi_R^{(-)}$ given by $\overline{E}=\omega-\epsilon_{B_1}$. The Pauli exclusion effects should be more important in $\chi_R^{(-)}$ than the P–T elastic coupling and will be approximated by the effective two-body cross section discussed below.

We next consider the inelastic part of the response function. As in equation (3), we expand $\overline{\boldsymbol{\Omega}}_{\mathbf{k}_1}^{(-)}$ into diagonal and off-diagonal parts. The off-diagonal terms correspond to inclusive reactions between $\mathbf{k}_1$ and the target recoil. The first term corresponds to $\mathbf{k}_1$ ejecting a second nucleon from the target where we are ignoring low-lying excited states. That term is given by

$$R_1^{\rm IN}(\mathbf{q},\mathbf{q}',\omega) = \int\frac{d\mathbf{k}_1}{(2\pi)^3}\ \frac{d\mathbf{k}_2}{(2\pi)^3}\ \delta\left(\omega-E_{\mathbf{k}_1}-E_{\mathbf{k}_2}\right)\int d\mathbf{r}\ d\mathbf{r}'\ e^{i\mathbf{q}\cdot\mathbf{r}}\ e^{-i\mathbf{q}'\cdot\mathbf{r}'}$$
$$\times\ e^{i\mathbf{k}_1\cdot(\mathbf{r}-\mathbf{r}')}\ \rho(\mathbf{r},\mathbf{r}')\ e^{\,i\left[\chi_R(\mathbf{s},z)-\chi_R^\dagger(\mathbf{s}',z')\right]}$$
$$\times\ <0_R\mid\widehat{\chi}_R(\mathbf{s},z)\mid\mathbf{k}_2><\mathbf{k}_2\mid\widehat{\chi}_R^\dagger(\mathbf{s}',z')\mid 0_R> \tag{44}$$

Using approximations similar to those made in equations (27), (42), and (43), we reduce equation (44) to

$$R_1^{\rm IN}(\boldsymbol{\alpha},\boldsymbol{\beta},\omega) = \left[\frac{\pi}{4}\left(w-\epsilon_{B_2}\right)\right]\frac{m_N\xi_2}{(2\pi)^2}\int d\mathbf{x}\ d\mathbf{y}\ e^{i\boldsymbol{\alpha}\cdot\mathbf{x}}\ e^{i\boldsymbol{\beta}\cdot\mathbf{y}}$$
$$\times\ \rho\left(\mathbf{y}+\frac{\mathbf{x}}{2},\mathbf{y}-\frac{\mathbf{x}}{2}\right)j_o(\xi_2 x)W_R^{(-)}(\mathbf{x},\mathbf{y},\xi_2) \tag{45}$$

where we define the collision term between recoil and nucleon knockouts as

$$W_R^{(-)}(\mathbf{x},\mathbf{y},\xi_2) = \frac{(A_T-1)}{(2\pi)^4\overline{\mathbf{k}}_{\rm NN}^2}\int_{x_z}^{\infty}dz\int_{y_z}^{\infty}dz'\int d^3\alpha'\ d^3\beta'\ e^{i\boldsymbol{\alpha}'\cdot\mathbf{x}(z)}\ e^{i\boldsymbol{\beta}'\cdot\mathbf{y}(z')}$$
$$\times\ \overline{\mathbf{f}}_{\rm NN}(\boldsymbol{\alpha}'+\boldsymbol{\beta}'/2)\overline{\mathbf{f}}_{\rm NN}^\dagger(\boldsymbol{\alpha}'-\boldsymbol{\beta}'/2)R_1^{\rm PW}(\boldsymbol{\alpha}',\boldsymbol{\beta}',\xi_2) \tag{46}$$

where $\mathbf{x}(z)=(\mathbf{x}_\perp,z)$ and $\mathbf{y}(z)=(\mathbf{y}_\perp,z')$. In equation (46) the plane-wave response function appears evaluated at the value ξ_2. Higher order terms in the intranuclear cascade could be added to the response function in equation (45) in a similar manner.

Method of Calculation and Results

By using shell model wave functions in a harmonic oscillator basis, the density matrix for $A_T \leq 40$ is found as

$$\rho\left(\mathbf{y}+\frac{\mathbf{x}}{2},\mathbf{y}-\frac{\mathbf{x}}{2}\right)=\frac{1}{\left(\pi R_T^2\right)^{3/2}}\,e^{-y^2/R_T^2}\,e^{-x^2/4R_T^2}\left\{a_s+2a_p\left(\frac{y^2}{R_T^2}-\frac{x^2}{4R_T^2}\right)\right.$$
$$\left.+\,a_d\left[\frac{3}{2}-\frac{2}{R_T^2}\left(\mathbf{y}^2+\frac{\mathbf{x}^2}{4}\right)+\frac{2}{R_T^4}\left(\mathbf{y}^2-\frac{\mathbf{x}^2}{4}\right)^2\right]\right\} \tag{47}$$

where the constant R_T represents the target matter radii and a_s, a_p, and a_d are occupation probabilities for s-, p-, and d-shell nucleons, respectively, given by (for $A_T \leq 40$)

$$a_s=\begin{cases}\frac{4}{A_T} & (A_T>4)\\ 1 & (A_T\leq 4)\end{cases} \tag{48}$$

$$3a_p=\begin{cases}0 & (A_T\leq 4)\\ \frac{A_T-4}{A_T} & (4>A_T\leq 16)\\ \frac{12}{A_T} & (A_T>16)\end{cases} \tag{49}$$

$$6a_d=\begin{cases}0 & (A_T\leq 16)\\ \frac{A_T-16}{A_T} & (A_T>16)\end{cases} \tag{50}$$

In equations (47)–(50) we treat the degenerate $1d$ and $2s$ shells approximately as a single shell, denoted d shell, because spin effects are not considered. In table I, values for shell-model occupation probabilities are given for several nuclei.

The plane-wave response function for the s shell is found by using equation (47) in equation (23) as

$$R_s=\frac{m_N a_s R_T}{\alpha\sqrt{\pi}}\,e^{-R_T^2\beta^2/4}\,e^{-R_T^2(\alpha^2+\xi^2)}\,\sinh\left(2R_T^2\alpha\xi\right) \tag{51}$$

Table I. Shell Model Parameters

Nucleus	a_s	a_p	a_d	[a] R_T, fm
^{4}He	1.0	0	0	1.33
^{6}Li	.57	.143	0	2.11
^{9}Be	.444	.185	0	1.79
^{12}C	.333	.222	0	1.69
^{16}O	.25	.25	0	1.83
^{20}Ne	.20	.20	.033	2.14
^{27}Al	.148	.148	.068	1.91
^{40}Ca	.1	.1	.1	2.10

[a] Values for R_T from references 1 and 16.

The plane-wave response function for the p-shell is found by

$$R_p = \frac{m_N a_p R_T}{\alpha\sqrt{\pi}} \left\{ \left[2 - \frac{1}{2}\ R_T^2\beta^2 + 2R_T^2\ (\alpha^2+\xi^2) \right]\ \sinh\left(2R_T^2\alpha\xi\right) \right.$$
$$\left. - 4R_T^2\ \alpha\xi \cosh\left(2R_T^2\alpha\xi\right) \right\}\ e^{-R_T^2\beta^2/4}\ e^{-R_T^2(\alpha^2+\xi^2)} \tag{52}$$

and the plane-wave response function for the d-shell is found by

$$R_d = \frac{m_N a_d R_T}{\alpha\sqrt{\pi}} \left\{ \left[\frac{7}{2} + 2R_T^2(\alpha^2+\xi^2) + 2R_T^4\ (\alpha^2+\xi^2)^2 \right.\right.$$
$$\left. + 8R_T^4\ \alpha^2\xi^2 \right]\ \sinh\left(2R_T^2\alpha\xi\right) - R_T^2\beta^2 \left[\frac{3}{2} + R_T^2(\alpha^2+\xi^2) \right]\ \sinh\left(2R_T^2\alpha\xi\right)$$
$$+\ \frac{1}{8}R_T^4\beta^4\ \sinh\left(2R_T^2\ \alpha\xi\right) - \left[4R_T^2\ \alpha\xi + 8R_T^4\ \alpha\xi(\alpha^2+\xi^2) \right] \cosh\left(2R_T^2\alpha\xi\right)$$
$$\left. + 2R_T^4\beta^2\alpha\xi\ \cosh\left(2R_T^2\ \alpha\xi\right) \right\}\ e^{-R_T^2\beta^2/4}\ e^{-R_T^2(\alpha^2+\xi^2)} \tag{53}$$

In an evaluation of the collision terms, the energy loss is taken as $\omega_i = \omega - \epsilon_{B_i}$, where ϵ_{B_i} is the separation energy corresponding to the orbit i. (See ref. 10.) Values for ϵ_{B_i} for a few nuclei are listed in table II as found in references 10 and 16. Analytic forms for R^{DW} and R^{IN} are not possible, so numerical integration is used.

Table II. Binding Energies of Shell Model Orbits

Nucleus	Orbit	[a] ϵ_{B_1}, MeV
^{4}He	s	20.5
^{6}Li	s	26.0
	p	5.2
^{9}Be	s	27.2
	p	18.2
^{12}C	s	38.7
	p	17.5
^{16}O	s	39.0
	p	18.0
^{27}Al	s	50.0
	p	22.0
	d	15.0
^{40}Ca	s	51.0
	p	35.0
	d	15.0

[a] Values for ϵ_{B_1} from references 10 and 16.

For $A_P \leq 4$ we use $F(q) = e^{-R_P^2 q^2/4}$, where the constant R_P represents the projectile matter radii. The two-body amplitude is parameterized as

$$f_{\mathrm{NN}} = \frac{\sigma(\rho + i)k_{\mathrm{NN}}}{4\pi} \, e^{-Bq^2/2} \tag{54}$$

where σ is the two-body cross section, B is the slope parameter, and ρ is the ratio of real to imaginary parts of the forward, two-body amplitude. Values for the two-body parameters are listed in table III for calculated versus laboratory (lab) energies.

Table III. NN Amplitude Parameters

T_{lab}, MeV	σ_{pp}, fm^2	σ_{np}, fm^2	B_{pp}, fm^2	B_{np}, fm^2	ρ_{pp}	ρ_{np}
558	3.85	3.58	0.12	0.12	0.40	−0.16
800	4.67	3.78	.16	.16	.18	−.33

In figures 1–3 we show the diagonal part ($\beta = 0$) of the response function for ^{4}He, ^{12}C, and ^{27}Al at several values of α versus the energy loss. Binding energies assumed for these nuclei are listed in table II. The multiple shell structures for ^{12}C and ^{27}Al are seen at lower values of α in figures 2 and 3. In figures 4–6 the off-diagonal part ($\beta \neq 0$) is displayed for $\alpha = 1.5$ fm^{-1}. The breaking of translational invariance in finite nuclei leads to a nonzero response for the off-diagonal components. Figures 4–6 show that the off-diagonal terms quickly dampen as we increase the target mass number, and the results for nuclear matter should be accurate for nuclei heavier than those considered here. Calculations that include ground-state correlations by Alberico et al. (ref. 17) also suggest that damping saturates at about $A_T = 40$. Figure 7 illustrates the complex structure of ^{27}Al caused by the multiple shell structure and the off-diagonal response.

The response terms with contributions for the FSI (eqs. (43) and (45)) contain the free two-body amplitude evaluated at an effective energy $\overline{E}$ that was determined by the projectile energy loss as $\overline{E} = w - \epsilon_{B_1}$. For the relatively low values of $\overline{E}$, we should expect significant deviations from the impulse approximation. We follow the usual approach of replacing the free two-body amplitude in equation (54) with an effective one that approximately treats some of the medium modifications. Smith and Bozoian (ref. 18) provide the parameterization

$$\bar{\sigma} = \left[\begin{array}{ll} \frac{2m_N}{P_L} \, \frac{100 \, T_L^2}{\left(T_L^2 + 18^2\right)} & (T_L \leq 164 \text{ MeV}) \\ \frac{2m_N}{P_L} \, 0.6 \, T_L & (T_L > 164 \text{ MeV}) \end{array} \right\} \tag{55}$$

where P_L and T_L are the nucleon kinetic momentum and energy, respectively, in the laboratory that correspond here to $\overline{E}$. The slope parameter is assumed as zero, which corresponds to the isotropic scattering that is approximately true at low energies. Equation (55) is based on optical potential studies. In reality, $\bar{\sigma}$ should contain a dependence on the target density and will differ for elastic or inelastic collision terms because the number of off-the-mass shell particles is not the same in these two cases.

Comparisons of the distorted-wave and inelastic response corrections with plane-wave response calculations are shown in figures 8–11 for ^{12}C. The DW response (dashed line) is lower than the PW response (solid line) at small values of α. The shapes of the response functions for the diagonal terms show only a slight shift in the position of the quasi-elastic peak because of

the inelastic term. In contrast, the off-diagonal contributions (figs. 10 and 11) are substantially modified. Here, the distorted waves alter the interference patterns because of the multiple shell structure. Calculations for heavier targets were not performed at this time because evaluations of inelastic response function are extremely complex for the higher shells.

Calculations of momentum spectra are shown in figures 12–15 at several angles along with comparisons with experimental data (ref. 19) for inclusive proton scattering on ^{6}Li, ^{12}C, ^{27}Al, and ^{40}Ca at a beam energy of 800 MeV. At the lowest momentum values, the effects of pion production are seen but are not included in our calculations. The calculations in figures 12–15 are made with the plane-wave response model and include contributions up to the fourth order. The second- and higher-order terms are small; however, these terms become more important with increasing target mass and momentum transfer. In figures 16 and 17, a similar comparison is made with the experimental data of reference 20 for protons at 558 MeV. Clearly, the dominant contribution for nucleon-nucleus collisions is the first collision term, which suggests that an improved description of the data will require going beyond the independent particle model used here to include correlation effects. This dominance of the first collision term contrasts with our previous results for composite projectiles (refs. 2 and 3) in which coherence effects are important for multiple scattering terms.

In figures 18 and 19, calculations are shown for ^{12}C and ^{27}Al that include the effects of final state interactions in the first-order response functions for 800-MeV proton beams. The inelastic collision term is seen to contribute to the distribution in a manner close to the plane-wave double collision term; this contribution is expected because the terms have the same dependence on energy loss and ground-state wave function. The combined effects of the distorted wave, ejectile, and recoil reduce the peak of the cross section with a slight shift in position. The inelastic collision term contributes primarily in the dip region between the quasi-elastic and pion production peaks.

Concluding Remarks

A formalism for describing the energy loss spectrum of fast ions in nuclear collisions at high energy was developed that includes the effects of final state interactions. Calculations in the independent particle model with harmonic oscillator wave functions suggest that a signature of the intranuclear cascade is seen in the dip region between the quasi-elastic and pion production peaks. The effects of the nuclear medium and the Pauli blocking are expected to be important in providing a more complete treatment of cascade effects than discussed in this paper. However, the present results indicate that cascade effects can be treated in an approach that is similar to the quantum mechanics used here.

NASA Langley Research Center
Hampton, VA 23681-0001
June 14, 1993

Appendix

Calculation of $\chi_R^{(-)}$

The outgoing distorted phase for the elastic coupling of the ejected nucleon with the core is written

$$\chi_R^{(-)}(\mathbf{y}) = \frac{(A_T - 1)}{(2\pi)^2 \overline{\mathbf{k}}_{\mathrm{NN}}^2} \int_{y_z}^{\infty} dz \int d^3q \; e^{i\mathbf{q}\cdot\mathbf{y}} \; G(\mathbf{q}) \bar{\mathrm{f}}_{\mathrm{NN}}(\mathbf{q}) \tag{A1}$$

The form factor is found from the one-body density matrix in equation (47) as

$$G(\mathbf{q}) = \left(C_1 + C_2 q^2 + C_3 q^4\right) \; e^{-R_T^2 q^2/4} \tag{A2}$$

where

$$C_1 = a_s + 3a_p + 6a_d = 1 \tag{A3}$$

$$C_2 = -R_T^2 \left(\frac{3}{4}\, a_p + 3a_d\right) \tag{A4}$$

$$C_3 = \frac{R_T^4}{8}\, a_p \tag{A5}$$

Using the two-body amplitude of equation (54), we have for the imaginary part of $\chi_R^{(-)}$

$$\mathrm{Im}\; \chi_R^{(-)}(\mathbf{y}) = \frac{(A_T - 1)\overline{\boldsymbol{\sigma}}}{(2\pi)^2 (4\pi)} \int_{y_z}^{\infty} dz \int d^3q \; e^{i\mathbf{q}\cdot\mathbf{y}} \left(C_1 + C_2 q^2 + C_3 q^4\right) \; e^{-wq^2} \tag{A6}$$

where

$$w = \frac{R_T^2}{4} + \frac{\overline{\mathbf{B}}}{2} \tag{A7}$$

Integration of equation (A5) leads to

$$\mathrm{Im}\; \chi_R^{(-)}(\mathbf{y}) = \frac{(A_T - 1)\overline{\boldsymbol{\sigma}}}{4w\sqrt{\pi}} \; e^{-y_\perp^2/4w} \left[A_1 \Gamma\left(\frac{1}{2}, y_z^2/4w\right) \right.$$

$$\left. + \, 4wA_2 \Gamma\left(\frac{3}{2}, \frac{y_z^2}{4w}\right) + 16w^2 A_3 \Gamma\left(\frac{5}{2}, \frac{y_z^2}{4w}\right) \right] \tag{A8}$$

where $\Gamma(a, u)$ is the incomplete gamma function defined by

$$\Gamma(a, u) = \int_u^{\infty} \; e^{-t} \; t^{a-1} \; dt \tag{A9}$$

and the coefficients A_1, A_2, and A_3 are defined as

$$A_1 = C_1 + \frac{C_2}{w}\left(\frac{3}{2} - \frac{y_\perp^2}{4w}\right) + \frac{C_3}{w^2}\left(\frac{15}{4} - \frac{5y_\perp^2}{4w} + \frac{y_\perp^4}{16w^2}\right) \tag{A10}$$

$$A_2 = -\frac{C_2}{4w^2} + \frac{C_3}{w^3}\left(-\frac{5}{4} + \frac{y_\perp^2}{8w}\right) \tag{A11}$$

and

$$A_3 = \frac{C_3}{16w^4} \tag{A12}$$

The energy variation of Im $\chi_R^{(-)}$ is through the two-body parameters $\overline{\sigma}$ and $\overline{\mathbf{B}}$ that are isospin averaged and evaluated at the energy $w - \epsilon_B$ in equation (43).

The coupling between the projectile and target can be evaluated from equation (A8) by replacing $(A_T - 1)$ with $A_P A_T$, letting $y_z \to -\infty$, using two-body parameters appropriate for the beam energy, and redefining w as

$$w = \frac{R_T^2}{4} + \frac{R_P^2}{4} + \frac{B}{2} \tag{A13}$$

where we assume a light projectile when a Gaussian form factor is sufficient.

References

1. Wilson, John W.; Townsend, Lawrence W.; Schimmerling, Walter; Khandelwal, Govind S.; Khan, Ferdous; Nealy, John E.; Cucinotta, Francis A.; Simonsen, Lisa C.; Shinn, Judy L.; and Norbury, John W.: *Transport Methods and Interactions for Space Radiations*. NASA RP-1257, 1991.

2. Cucinotta, Francis A.; Townsend, Lawrence W.; and Wilson, John W.: *Quasi-Elastic Nuclear Scattering at High Energies*. NASA TM-4362, 1992.

3. Cucinotta, Francis A.; Townsend, Lawrence W.; and Wilson, John W.: Multiple-Scattering Effects in Quasielastic $\alpha-{}^4$He Scattering. *Phys. Review C*, vol. 46, no. 4, Oct. 1992, pp. 1451–1456.

4. West, Geoffrey B.: Electron Scattering From Atoms, Nuclei and Nucleons. *Phys. Rep.*, vol. 18 C, no. 5, June 1975, pp. 263–323.

5. Sick, I.; Day, D.; and McCarthy, J. S.: Nuclear High-Momentum Components and y Scaling in Electron Scattering. *Phys. Review Lett.*, vol. 45, no. 11, Sept. 15, 1980, pp. 871–874.

6. Gurvitz, S. A.; and Rinat, A. S.: y Scaling in Inclusive Scattering. *Phys. Review C*, third ser., vol. 35, no. 2, Feb. 1987, pp. 696–707.

7. Lee, T.-S. H.; and Miller, G. A.: Color Transparency and High-Energy (p, 2p) Nuclear Reactions. *Phys. Review C*, third ser., vol. 45, no. 4, Apr. 1992, pp. 1863–1870.

8. Brodsky, Stanley J.; and de Teramond, Guy F.: Spin Correlations, QCD Color Transparency, and Heavy-Quark Thresholds in Proton-Proton Scattering. *Phys. Review Lett.*, vol. 60, no. 19, May 9, 1988, pp. 1924–1927.

9. Jennings, B. K.; and Miller, G. A.: Energy Dependence of Color Transparency. *Phys. Review D*, third ser., vol. 44, no. 3, Aug. 1, 1991, pp. 692–703.

10. Horikawa, Y.; Lenz, F.; Mukhopadhyay, Nimai C.: Final-State Interaction in Inclusive Electromagnetic Nuclear Processes. *Phys. Review C*, third ser., vol. 22, no. 4, Oct. 1980, pp. 1680–1695.

11. Wilson, John W.: *Composite Particle Reaction Theory*. Ph.D. Diss., College of William and Mary in Virginia, June 1975.

12. Feshbach, H.; and Hüfner, J.: On Scattering by Nuclei at High Energies. *Ann. Phys.*, vol. 56, no. 1, Jan. 1970, pp. 268–294.

13. Cucinotta, Francis A.: Theory of Alpha-Nucleus Collisions at High Energies. Ph.D. Thesis, Old Dominion Univ., 1988.

14. Krimm, H.; Klar, A.; and Pirner, H. J.: Inelastic Scattering of Fast Particles on Nuclei. *Nucl. Phys.*, vol. A367, no. 3, Sept. 14, 1981, pp. 333–357.

15. Cucinotta, Francis A.; Townsend, Lawrence W.; and Wilson, John W.: Inclusive Inelastic Scattering of Heavy Ions in the Independent Particle Model. *J. Phys. G: Nucl. Particle Phys.*, vol. 18, no. 5, May 1992, pp. 889–901.

16. Barrett, Roger C.; and Jackson, Daphne F.: *Nuclear Sizes and Structure*. Oxford Univ. Press, 1979.

17. Alberico, W. M.; Molinari, A.; De Pace, A.; Ericson, M.; and Johnson, Mikkel B.: Random Phase Approximation Spin-Isospin Nuclear Response in the Deep Inelastic Region. *Phys. Review C*, third ser., vol. 34, no. 3, Sept. 1986, pp. 977–990.

18. Smith, R. D.; and Bozoian, M.: Quasifree Scattering in the Preequilibrium Region. *Phys. Review C*, third ser., vol. 39, no. 5, May 1989, pp. 1751–1760.

19. Chrien, R. E.; Krieger, T. J.; Sutter, R. J.; May, M.; Palevsky, H.; Stearns, R. L.; Kozlowski, T.; and Bauer, T.: Proton Spectra From 800 MeV Protons on Selected Nuclides. *Phys. Review C*, third ser., vol. 21, no. 3, Mar. 1980, pp. 1014–1029.

20. Beck, Sherwin M.; and Powell, Clemans A.: *Proton and Deuteron Double Differential Cross Sections at Angles From 10° to 60° From Be, C, Al, Fe, Cu, Ge, W, and Pb Under 558 MeV-Proton Irradiation*. NASA TN D-8119, 1976.

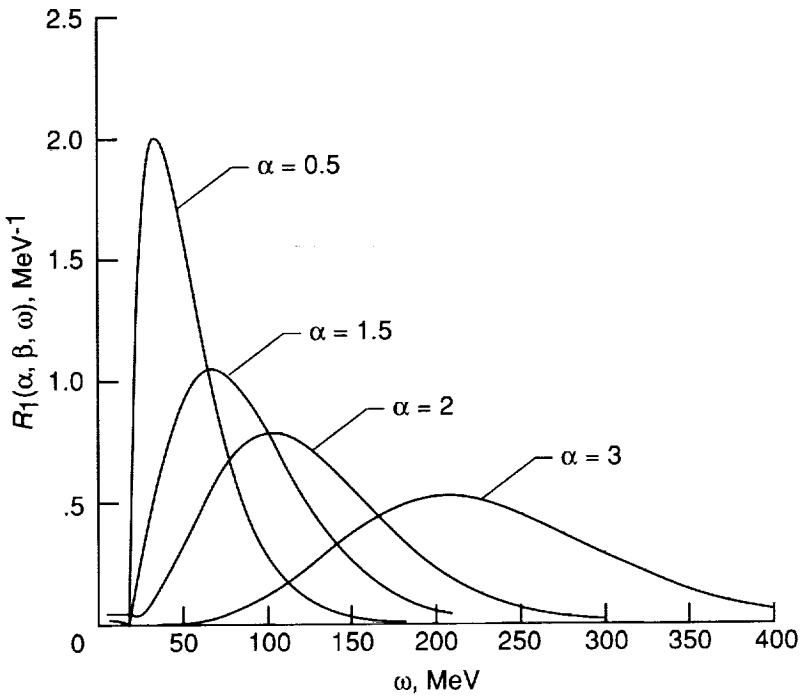

Figure 1. Diagonal part of first-order response function versus energy loss for ^{4}He with $\beta = 0$. All dimensions are in fm^{-1}.

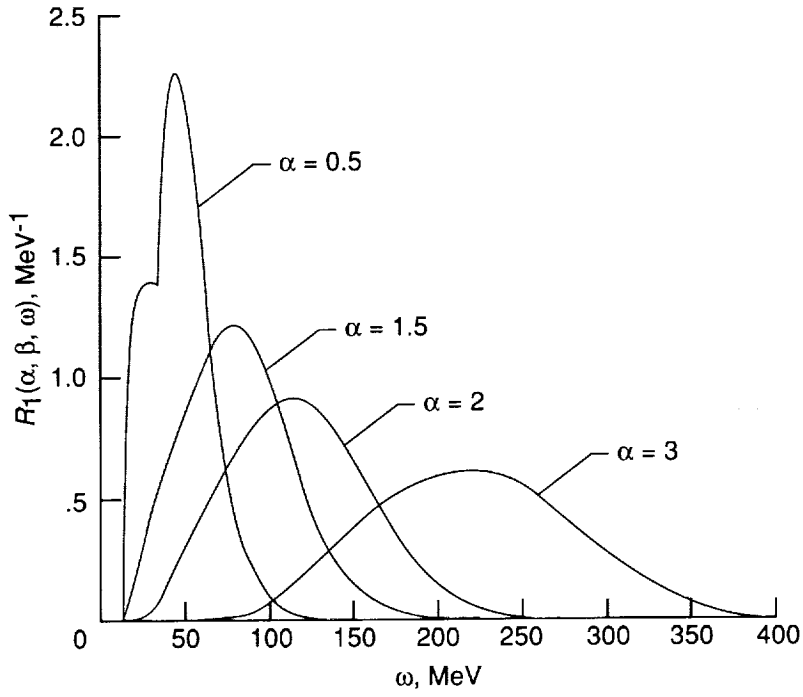

Figure 2. Diagonal part of first-order response function versus energy loss for ^{12}C with $\beta = 0$. All dimensions are in fm^{-1}.

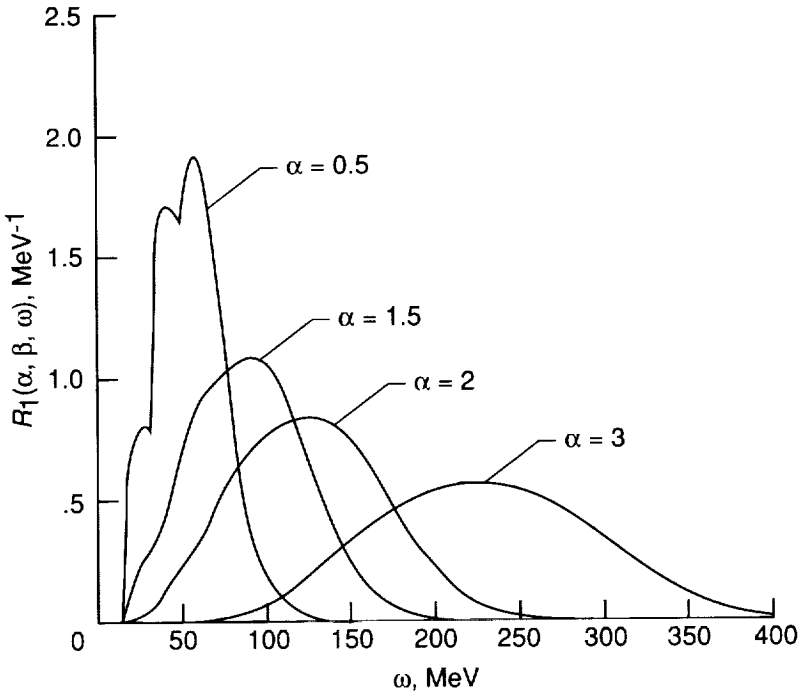

Figure 3. Diagonal part of first-order response function versus energy loss for ^{27}Al with $\beta = 0$. All dimensions are in fm^{-1}.

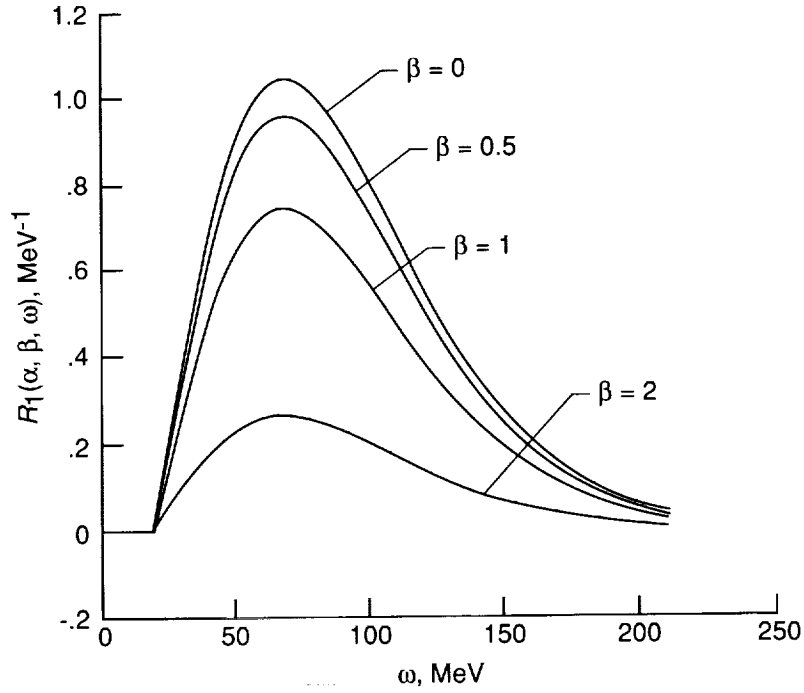

Figure 4. Off-diagonal part of first-order response function versus energy loss for ^{4}He at $\alpha = 1.5$ fm^{-1} and several values of β. All dimensions are in fm^{-1}.

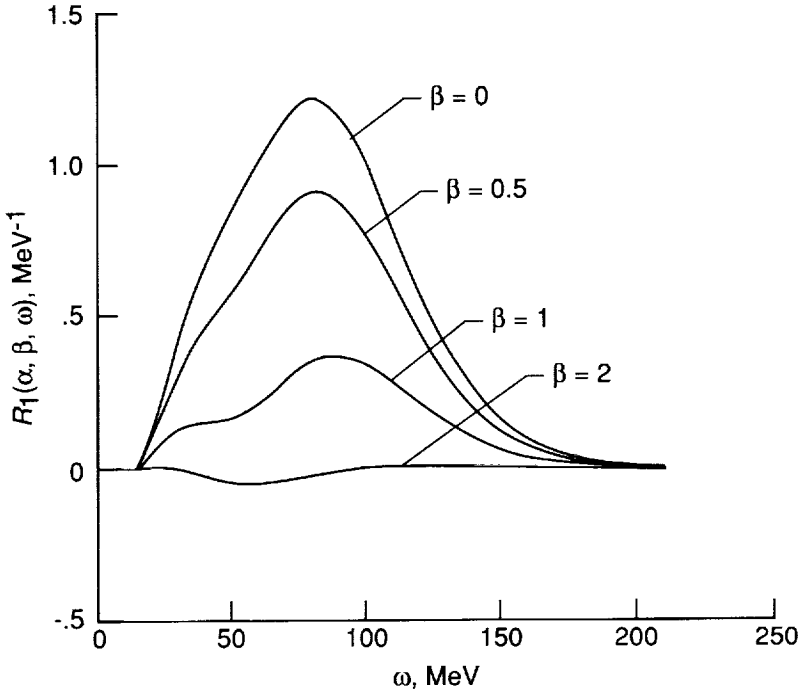

Figure 5. Off-diagonal part of first-order response function versus energy loss for ^{12}C at $\alpha = 1.5$ fm^{-1} and several values of β. All dimensions are in fm^{-1}.

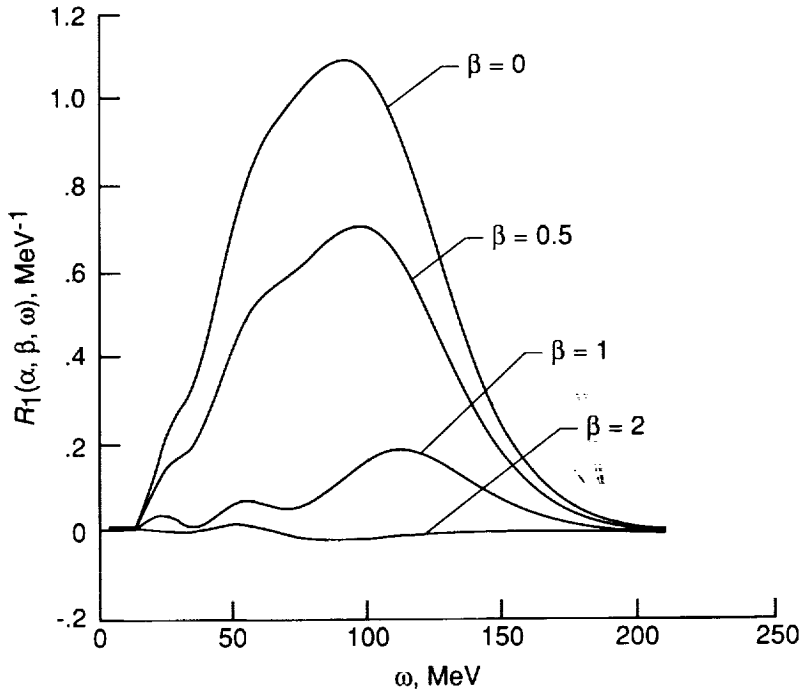

Figure 6. Off-diagonal part of first-order response function versus energy loss for ^{27}Al at $\alpha = 1.5$ fm^{-1} and several values of β. All dimensions are in fm^{-1}.

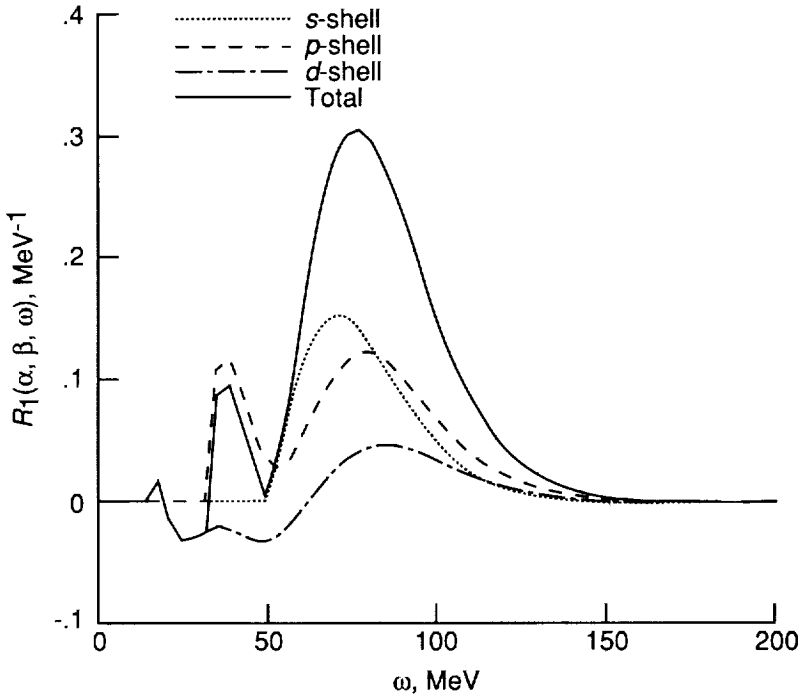

Figure 7. Off-diagonal part of first-order response function versus energy loss for ^{27}Al with contributions from individual shells. $\alpha = \beta = 1$ fm^{-1}.

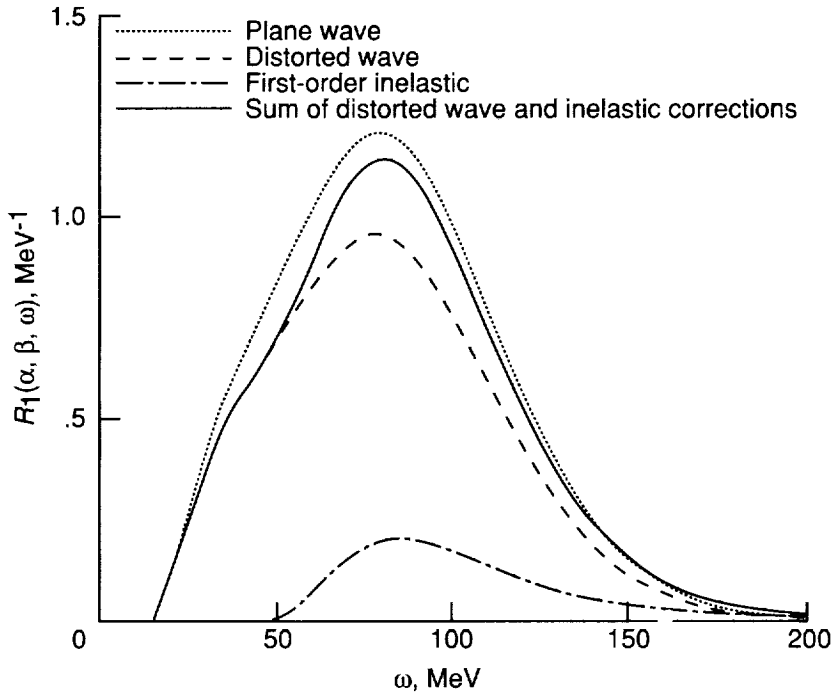

Figure 8. Diagonal part of first-order response function for ^{12}C with inelastic corrections. $\alpha = 1.5$ fm^{-1}; $\beta = 0$ fm^{-1}.

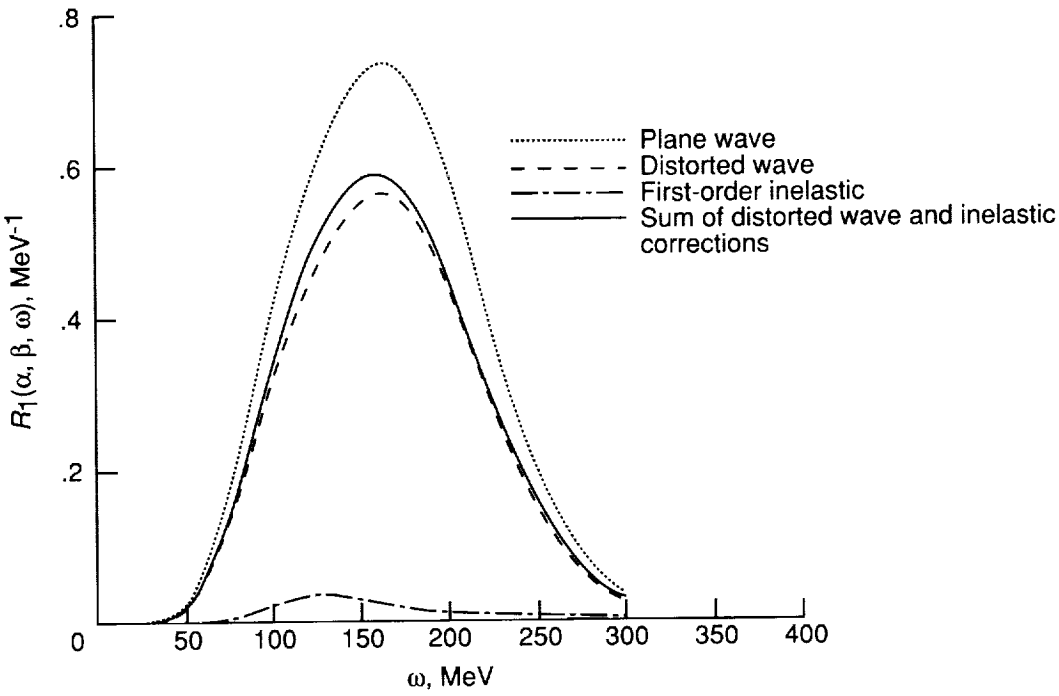

Figure 9. Diagonal part of first-order response function for larger momentum transfer with inelastic corrections. $\alpha = 2.5$ fm^{-1}; $\beta = 0$ fm^{-1}.

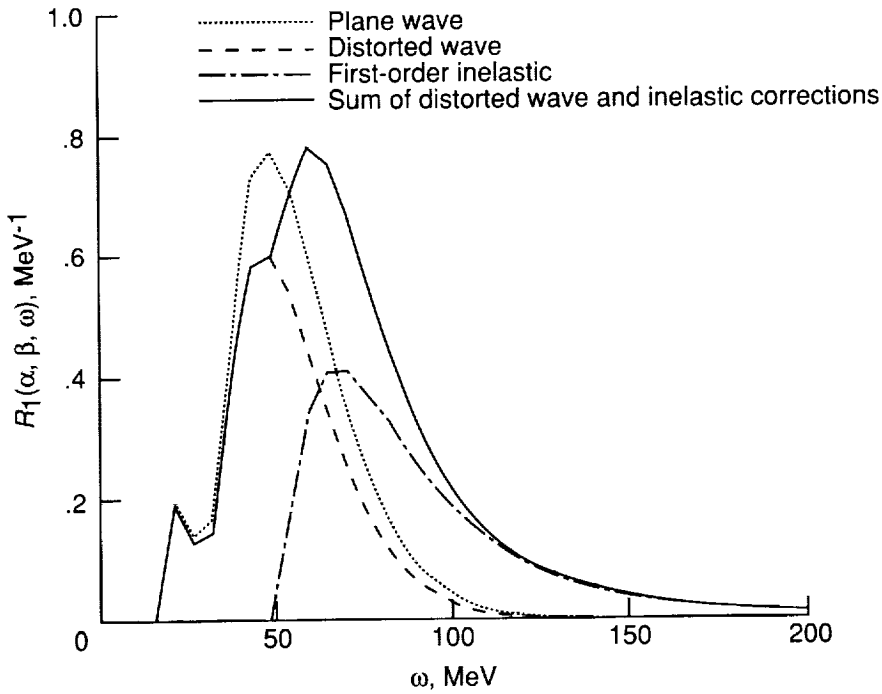

Figure 10. Off-diagonal part of first-order response function with inelastic corrections. $\alpha = 0.75$ fm^{-1}; $\beta = 1$ fm^{-1}.

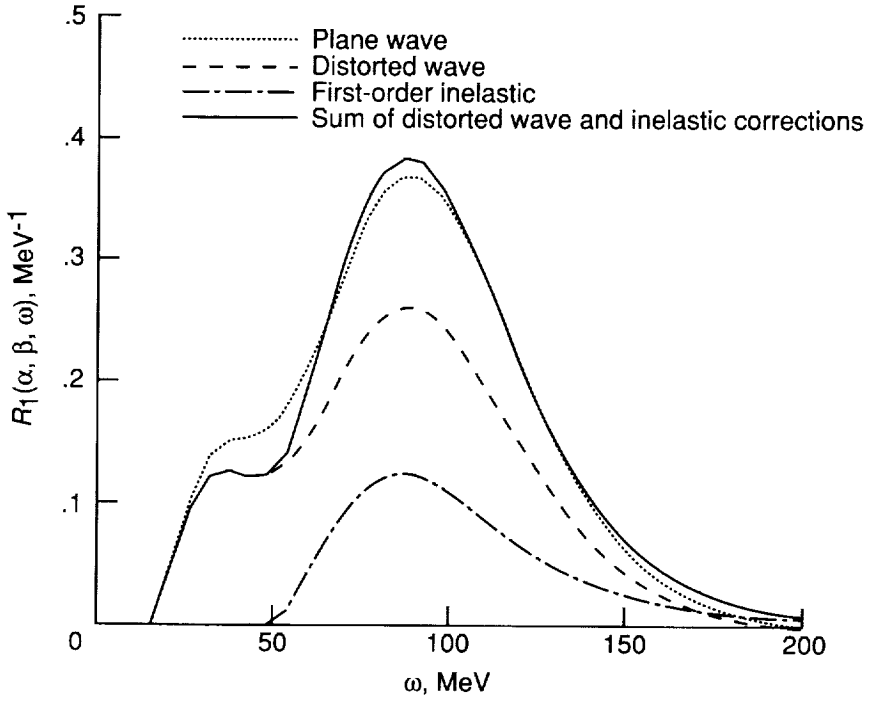

Figure 11. Off-diagonal part of first-order response function with inelastic corrections. $\alpha = 1.5$ fm^{-1}; $\beta = 1$ fm^{-1}.

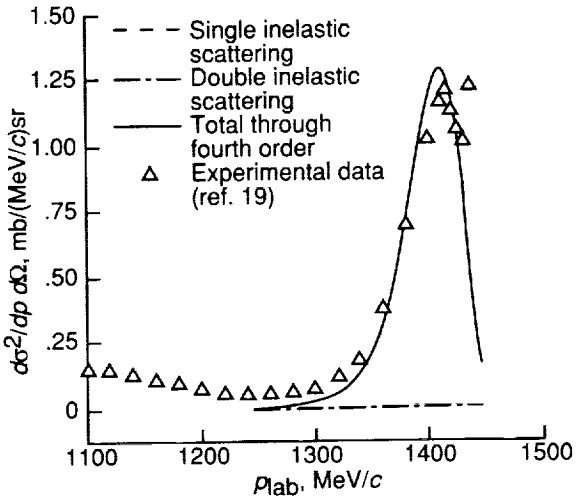

(a) $\Theta = 11°$.

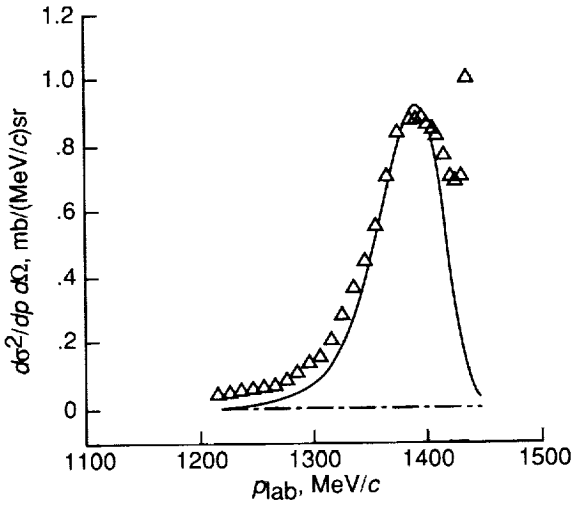

(b) $\Theta = 13°$.

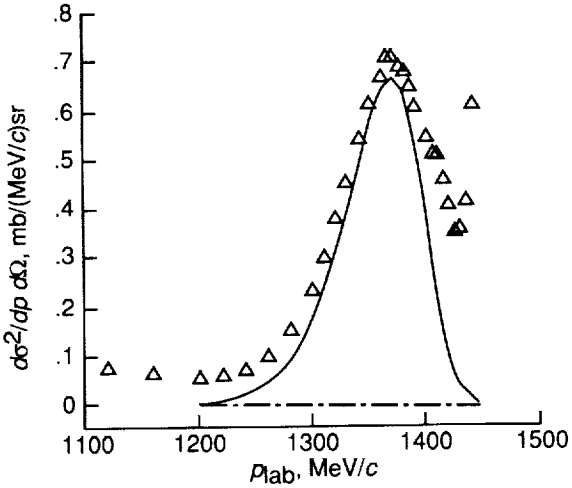

(c) $\Theta = 15°$.

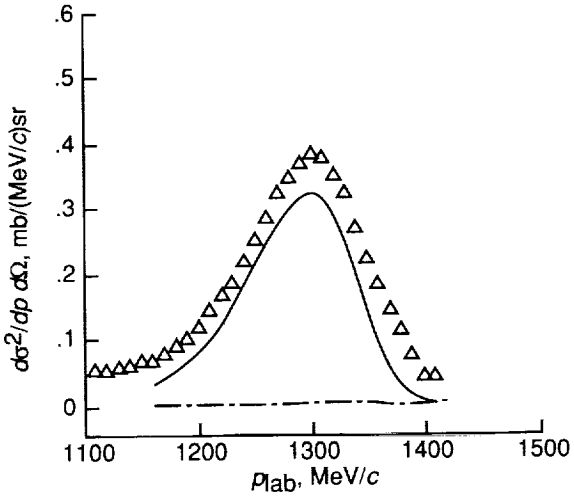

(d) $\Theta = 20°$.

Figure 12. Calculations of inclusive p scattering for ^{6}Li at 800 MeV compared with data of reference 19. $p + {}^6\mathrm{Li} \rightarrow p + \mathrm{X}$ at 800 MeV.

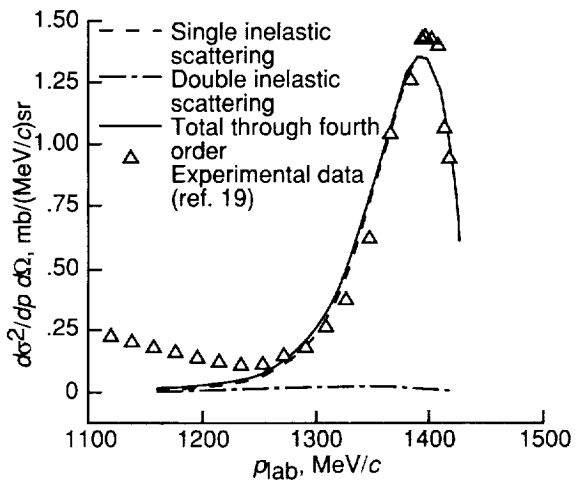

(a) $\Theta = 11°$.

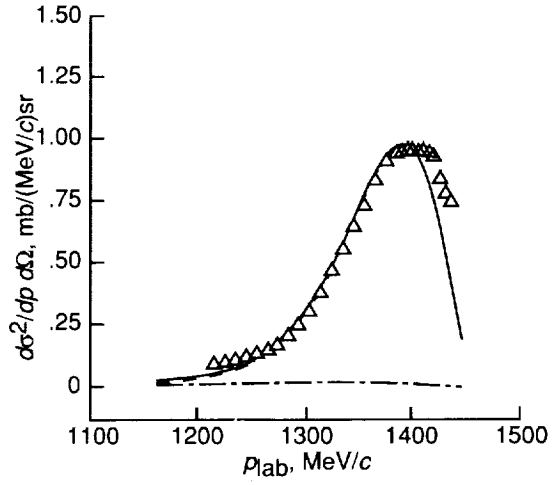

(b) $\Theta = 13°$.

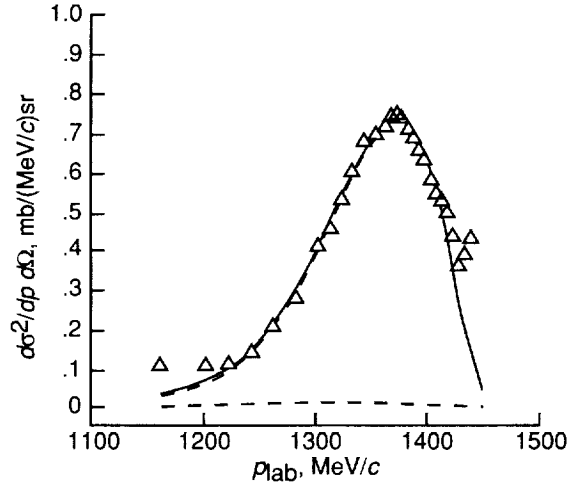

(c) $\Theta = 15°$.

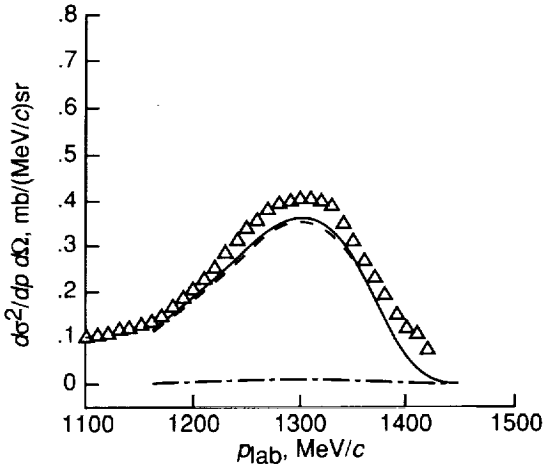

(d) $\Theta = 20°$.

Figure 13. Calculations of inclusive p scattering for ^{12}C at 800 MeV compared with data of reference 19. $p + {}^{12}C \rightarrow p + X$ at 800 MeV.

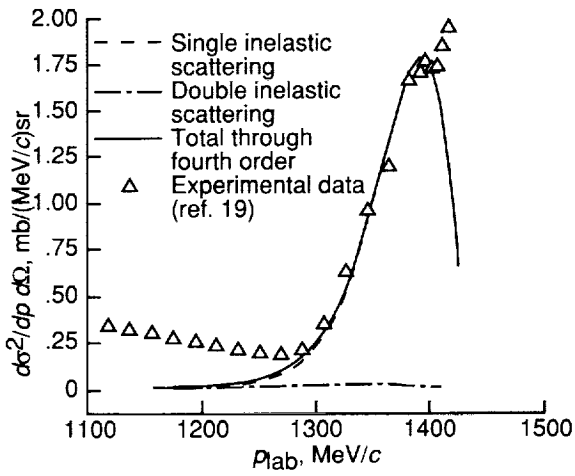

(a) $\Theta = 11°$.

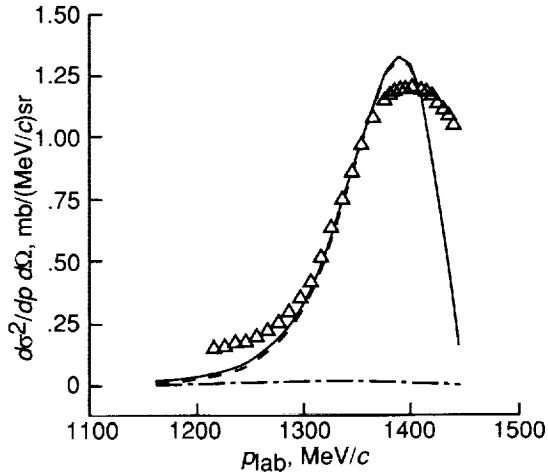

(b) $\Theta = 13°$.

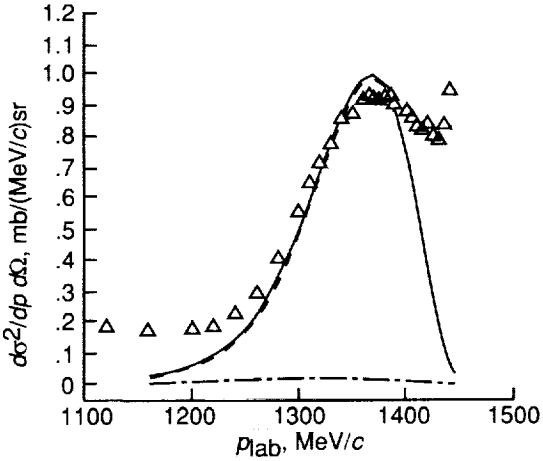

(c) $\Theta = 15°$.

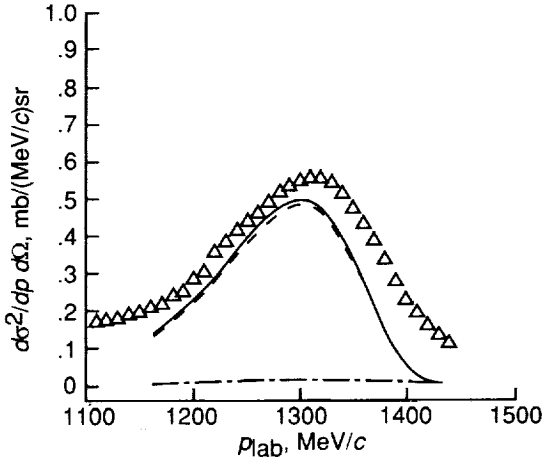

(d) $\Theta = 20°$.

Figure 14. Calculations of inclusive p scattering for ^{27}Al at 800 MeV compared with data of reference 19. $p + {}^{27}\mathrm{Al} \rightarrow p + \mathrm{X}$ at 800 MeV.

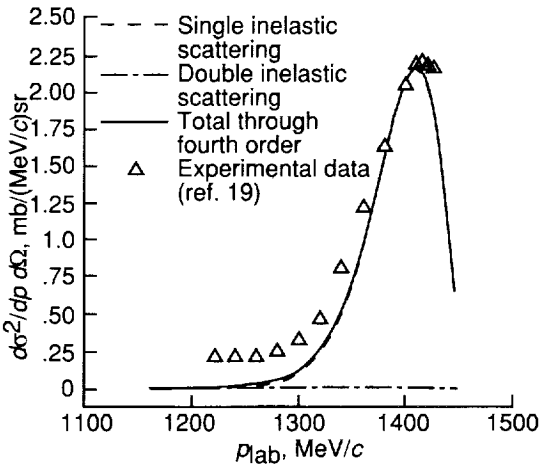

(a) $\Theta = 11°$.

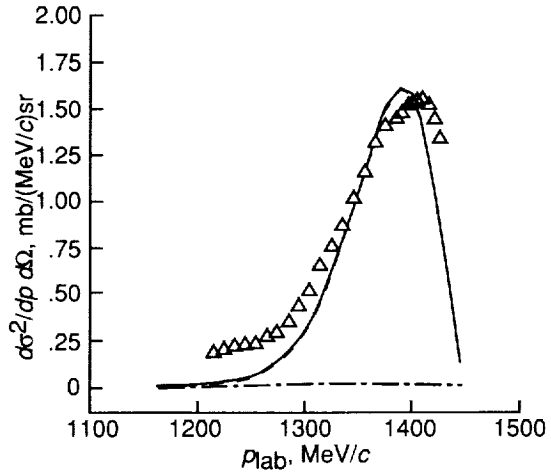

(b) $\Theta = 13°$.

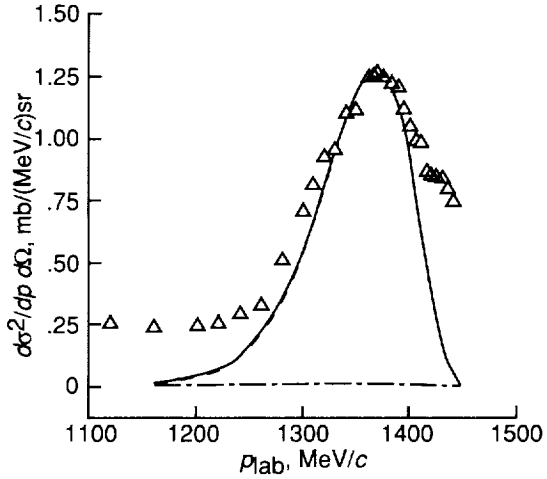

(c) $\Theta = 15°$.

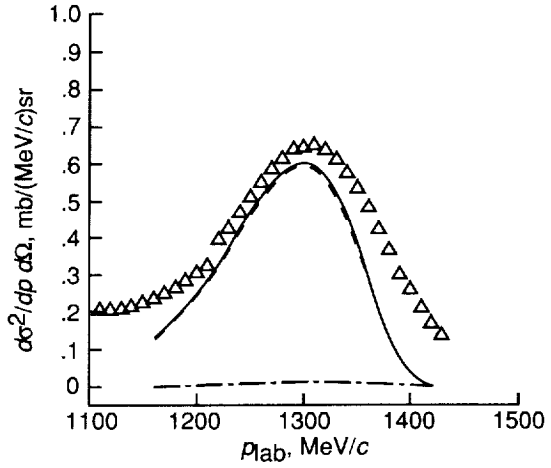

(d) $\Theta = 20°$.

Figure 15. Calculations of inclusive p scattering for ^{40}Ca at 800 MeV compared with data of reference 19. $p + {}^{40}\mathrm{Ca} \rightarrow p + \mathrm{X}$ at 800 MeV.

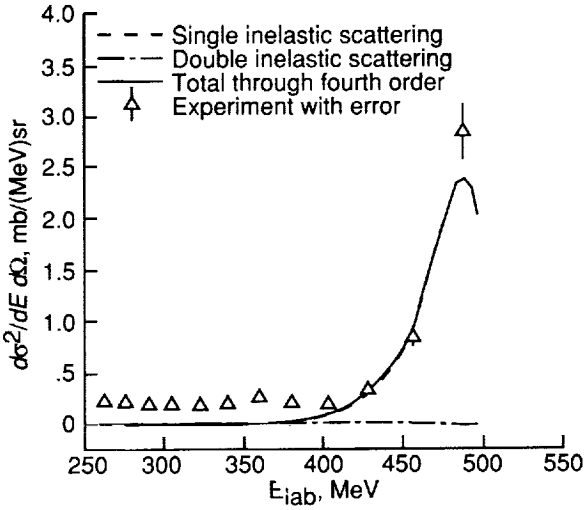

(a) $\Theta = 10°$.

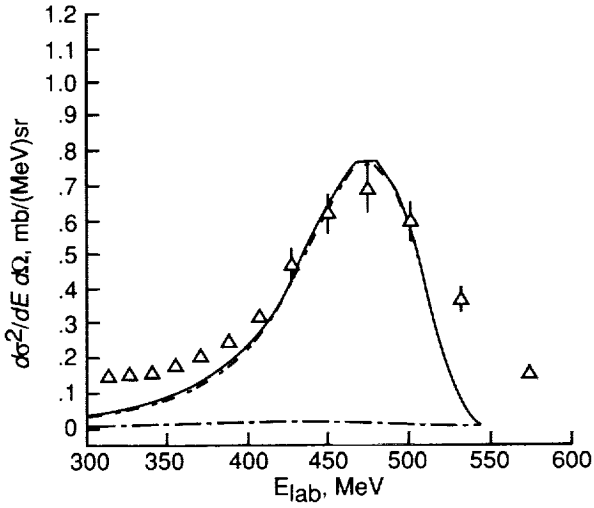

(b) $\Theta = 20°$.

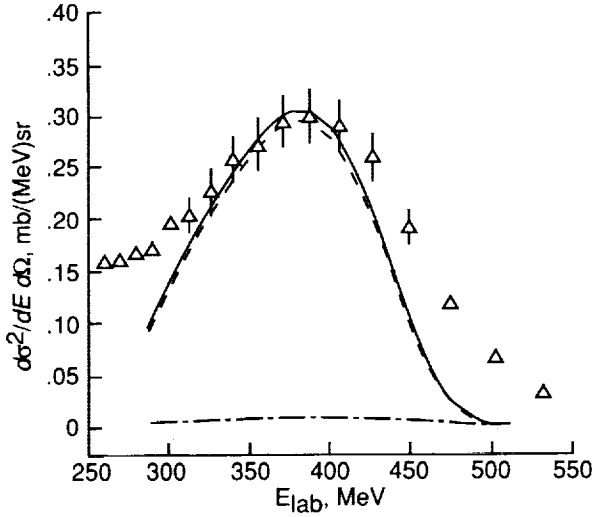

(c) $\Theta = 30°$.

Figure 16. Calculations of inclusive p scattering for ^{12}C at 558 MeV compared with data of reference 20. $p + {}^{12}\mathrm{C} \rightarrow p + \mathrm{X}$ at 558 MeV.

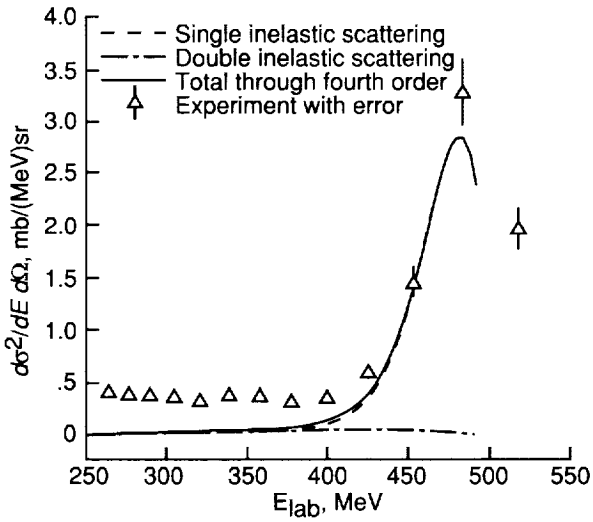

(a) $\Theta = 10°$.

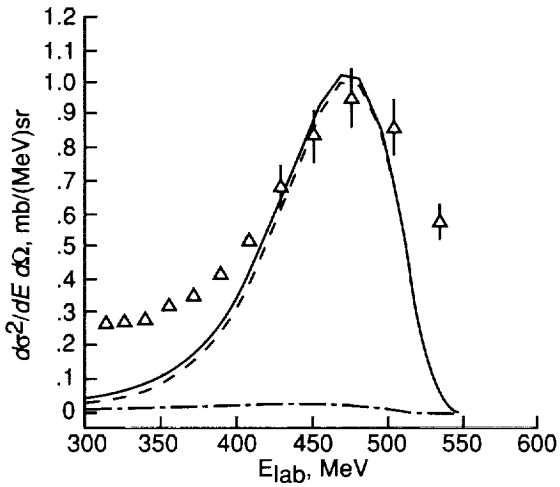

(b) $\Theta = 20°$.

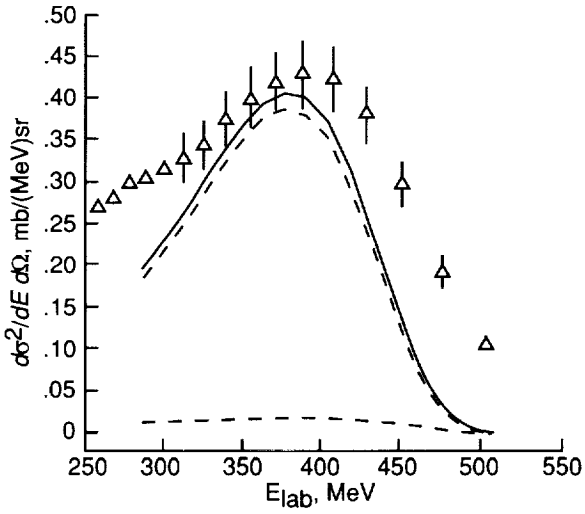

(c) $\Theta = 30°$.

Figure 17. Calculations of inclusive p scattering for ^{27}Al at 558 MeV compared with data of reference 20. $p + {}^{27}\mathrm{Al} \rightarrow p + \mathrm{X}$ at 558 MeV.

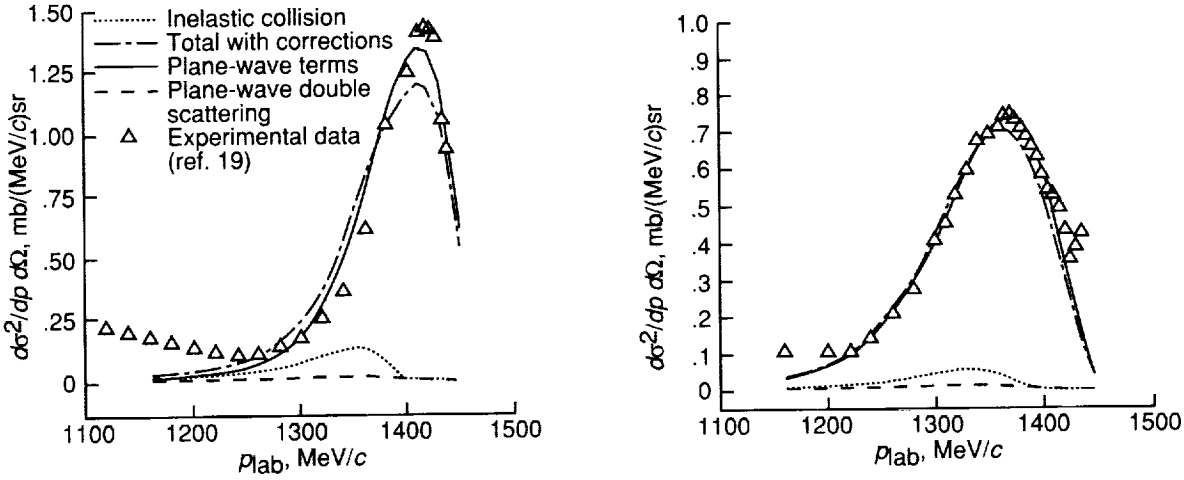

(a) $\Theta = 11°$.

(b) $\Theta = 15°$.

Figure 18. Calculations of inclusive p scattering for ^{12}C at 800 MeV that include final state interactions. Experimental data from reference 19. $p + {}^{12}C \rightarrow p + X$ at 800 MeV.

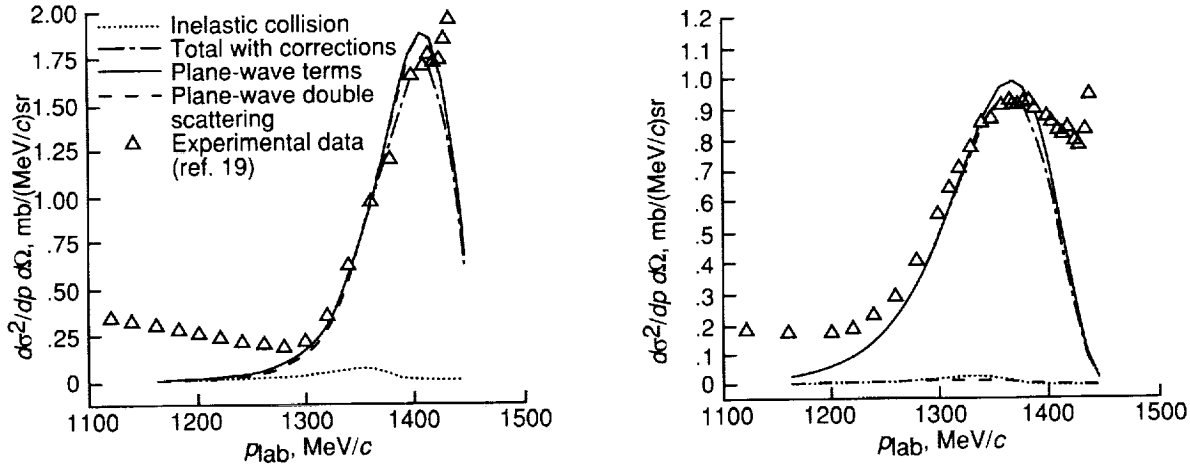

(a) $\Theta = 11°$.

(b) $\Theta = 15°$.

Figure 19. Calculations of inclusive p scattering for ^{27}Al at 800 MeV that include final state interactions. Experimental data from reference 19. $p + {}^{12}C \rightarrow p + X$ at 800 MeV.

REPORT DOCUMENTATION PAGE

Form Approved
OMB No. 0704-0188

1. AGENCY USE ONLY *(Leave blank)*	2. REPORT DATE	3. REPORT TYPE AND DATES COVERED
	August 1993	Technical Paper

4. TITLE AND SUBTITLE
Final State Interactions and Inclusive Nuclear Collisions

5. FUNDING NUMBERS
WU 199-45-16-11

6. AUTHOR(S)
Francis A. Cucinotta and Rajendra R. Dubey

7. PERFORMING ORGANIZATION NAME(S) AND ADDRESS(ES)
NASA Langley Research Center
Hampton, VA 23681-0001

8. PERFORMING ORGANIZATION REPORT NUMBER
L-17240

9. SPONSORING/MONITORING AGENCY NAME(S) AND ADDRESS(ES)
National Aeronautics and Space Administration
Washington, DC 20546-0001

10. SPONSORING/MONITORING AGENCY REPORT NUMBER
NASA TP-3353

11. SUPPLEMENTARY NOTES
Cucinotta: Langley Research Center, Hampton, VA; Dubey: Old Dominion University, Norfolk, VA.

12a. DISTRIBUTION/AVAILABILITY STATEMENT
Unclassified Unlimited

Subject Category 73

12b. DISTRIBUTION CODE

13. ABSTRACT *(Maximum 200 words)*
A scattering formalism is developed in a multiple scattering model to describe inclusive momentum distributions for high-energy projectiles. The effects of final state interactions on response functions and momentum distributions are investigated. Calculations for high-energy protons that include shell model response functions are compared with experiments.

14. SUBJECT TERMS
Nuclear reactions; Multiple scattering models; High-energy protons; Cosmic rays

15. NUMBER OF PAGES
29

16. PRICE CODE
A03

17. SECURITY CLASSIFICATION OF REPORT	18. SECURITY CLASSIFICATION OF THIS PAGE	19. SECURITY CLASSIFICATION OF ABSTRACT	20. LIMITATION OF ABSTRACT
Unclassified	Unclassified		